MICOS Complex and Mitochondria Morphology Changes Across Aging in Cardiac Muscle

Zer Vue[1*], Edgar Garza-Lopez[2*], Kit Neikirk[1*], Larry Vang[1], Heather Beasley[1], Amber Crabtree[1], Andrea G. Marshall[1], Sandra Murray[3], Antentor Hinton, Jr[1#]

[1] Department of Molecular Physiology and Biophysics, Vanderbilt University, Nashville, TN, 37232, USA.
[2] Department of Internal Medicine, University of Iowa, Iowa City, IA, 52242, USA.
[3]Department of Cell Biology, University of Pittsburgh, Pittsburgh, PA 15261, USA.

*These authors share co-first authorship.
#These authors share senior authorship.

Corresponding Author:
Antentor Hinton
Department of Molecular Physiology and Biophysics
Vanderbilt University
antentor.o.hinton.jr@Vanderbilt.Edu 319-383-3095

ABSTRACT: Cardiac disease remains a large cause of death among humans and therapies to treat it remain lacking. Mitochondria is heavily implicated in various critical functions of the cell not limited to the production of ATP. Critically, mitochondria break down across aging and heart also decrease in efficiency in aging. Key factors implicated in mitochondria morphology, such as the mitochondrial contact site and cristae organizing system (MICOS), role across aging remains to be seen in cardiac muscle. To better understand the relationship between mitochondria in heart, we used transmission electron microscopy (TEM) and serial block facing-scanning electron microscopy (SBF-SEM) to quantitatively analyze the 3D networks in cardiac muscle samples of mice at aging intervals. Cardiac muscle showed some breaking down across aging, decreased areas, increased mitochondria, but less fragmentation and wide-spread changes across 2-year aging than previous studies in skeletal muscle. In studying cristae, the inner folds of mitochondria, we observed a loss of morphology across aging. This mimicked what was observed upon CRISPR/Cas9 knockdown of *mitofilin*, *Chchd3*, *Chchd6* and *Opa-1* which showed increased lamellar cristae and fragmented mitochondria while mitochondria length and volume decreased. We are the first to examine mitochondria changes in cardiac muscle across aging. Notably, we noticed differences in skeletal muscle, which we have previously studied, and cardiac muscle that suggests a differential response to mitochondrial aging in cardiac and skeletal muscle. In combination, these data suggest that, in the heart, loss of the MICOS complex may be implicated in the loss of function in mitochondria that is seen across aging.

INTRODUCTION:

The mitochondria is an organelle that critically carries out oxidative phosphorylation in the cell, and is implicated in many disease states including Alzheimer's, diabetes, and heart failure [1–3]. Given the dependence on mitochondria for the energy, deterioration or loss of

function in mitochondria can be associated with failure of cells and states including autophagy, in some cases, and apoptosis [4–6]. Beyond only being responsible for producing adenosine triphosphate (ATP), mitochondria also are involved in cell signaling, through calcium homeostasis; programmed cell death, apoptosis; and regulate immunity, through signaling that determines immune cell function [5,7–9]. Interestingly, previous research has also suggested that mitochondria is implicated in aging [10,11]. The mitochondrial free radical theory of aging (MRFTA) proposes this mechanism arises as a result of degradation by of reactive oxygen species, which are oxidative phosphorylation byproducts [10,12]. While many of the functions of mitochondria have been studied before, the specific changes and causes of changes in mitochondria across aging is still poorly understood, as is how this could be linked to disease states.

Key to mitochondria function is the morphology. Mitochondria undergo dynamics of fusion and fission which are regulated by optic atrophy 1 (OPA-1) and dynamin related protein-1 (DRP-1), respectively [4,13–15]. While loss of DRP-1 results in an abundance of mitochondria that fuse together and are overly elongated [5], loss of OPA-1 results in mitochondria that are fragmented [13,16]. Beyond this, loss of either of these critical genes also impact mitochondrial cristae [14,17]. Cristae are folds of the mitochondria inner-membrane that have electron transfer chain complexes which are responsible for ATP synthesis [18]. Critically, the morphology of cristae can be critical in their energetic efficiency [18]. Beyond this, cristae morphology has also been implicated in other functions of mitochondria [18]. For cristae, the shape can present different outcomes in mitochondria, and cristae can be seen as either lamellar, during which they present as flat sacs, or tubular, during which they resemble tubes [19]. Typically, cristae dynamically have populations of both lamellar and tubular cristae. However, recent research has suggested that lamellar cristae does not require mitochondrial fusion, so therefore they may be able to form independent of OPA-1, or in states of OPA-1 deficiency [20]. Lamellar cristae is more accommodating of increases in volume, and have been suggested that they increase in prominence as cristae fusion occurs during mitochondria stress states [21].

Critical in the regulation of both of these formations of cristae types is the mitochondrial contact site and cristae organizing system (MICOS). Similar to OPA-1, the MICOS complex regulates changes in the cristae, as cristae show continuous changes [17,22–24]. The MICOS complex is made up of several key genes that are critical in maintaining the morphology of both cristae and mitochondria [24]. Beyond only regulating the shape of cristae, maintenance of junctions in the cristae, which act as sub compartments for mitochondria as barriers for metabolites, is also controlled by the MICOS complex [25]. Given the importance of the cristae junctions, this may also implicate cristae in calcium homeostasis and molecular signaling. Given the implication of mitochondria and cristae morphology in function, alterations in the MICOS complex could further impact health [23]. Specifically, it still remains unknown how the MICOS complex affects aging and mitochondria health in the heart. Given past research that has suggested mitochondria is affected by aging [11], we hypothesized that this change may come as a result of changes in the MICOS complex, which are critical to maintaining mitochondrial and cristae morphology [20,26].

We have specifically sought to study cardiac muscle in mouse because it remains a novel target that has implications for mitochondria health of the heart. This study combines an *in vivo* and *in vitro* approach by both looking at cardiac muscle in mouse and fibroblasts. Previously, aging has been studied in cardiomyocytes [27]; however, these studies have not considered the MICOS complex in relation to this aging of the cardiomyocytes. Cardiac health is heavily

implicated with insulin-resistance and is linked to diabetes [1,28]. Importantly, heart failure has also been linked to factors including endoplasmic reticulum stress, mitochondrial bioenergetics, insulin signaling, autophagy, and oxidative stress [29], which are all factors which the mitochondria plays a role in [6,30–32]. Mitochondria show specialization in types and structures associated with their roles in glycolysis and oxidative metabolism in cardiomyocytes [33–36]. While young mitochondria show extensive specialization, it is not known whether this is true for aged mitochondria, there is little information on whether the impact of aging regulates mitochondrial genes that affect structure. In cardiac muscle, past research has found that across aging, mitochondria in between myofibrils, called interfibrillar mitochondria, show the largest decrease in mitochondria function [37]. However, it remains to be seen what caused these changes in the oxidative phosphorylation of interfibrillar mitochondria. Given that heart failure increases across aging as heart function is loss [38], mitochondria may contribute to this [29]. Therefore, mitochondria in the heart represent a critical target for therapies aimed at cardiac diseases, heart failure, and diabetes.

To better understand the relationship between mitochondria in heart, we used transmission electron microscopy (TEM) for 2D micrographs to observe cristae. We also used serial block facing-scanning electron microscopy (SBF-SEM) to quantitatively analyze the 3D networks in cardiac muscle samples of mice at aging intervals. With this high-resolution technique, we were able to look at single-organelle resolution and compared shape, morphology, amount, networking, and branching across age points. To further understand how aging affected the morphology, we looked at mitochondria and cristae at three time points, 3-month, 1-year, and 2-year which represent "young," "middle-aged," and "old," mouse respectively. We have previously performed this method in skeletal muscle. Previous research has shown that cardiac and skeletal muscle differ [33,34], but this is not yet known how this changes across aging. Furthermore, we also looked at the impact of aging in MICOS genes. Critically, in this study, we used CRISPR/Cas9 editing to individually knockout (KO) three genes of the MICOS complex, and *Chchd3* (*Mic19*), *Chchd6* (*Mic25*), *Mitofilin* (*Mic60*), as well as *Opa-1* and examined mitochondria through fluorescence and 3D reconstruction. Finally, we also observed KO of the MICOS complex genes and *Opa-1* through 3D reconstruction in cardiac fibroblasts.

RESULTS:

TEM Shows Changes in Mitochondria and Cristae Across Aging

We began by examining mitochondria and cristae morphology in cardiac muscle across 3-month, 1 year, and 2-year-old mouse. Studying cardiac muscle allows if mitochondria morphological changes are exclusive to skeletal muscle, since cardiac muscle allows for the comparison to different types of cells [36], and cardiac muscle can give information about potential causes of loss of optimal function in heart across aging [38]. TEM is useful as it gives very high quality micrographs which allow for viewing of cristae and identification of mitochondria [39]. While the young male mouse show very clearly mitochondria with electron dense membranes and clear membranes, the aged mouse show less clear mitochondria and cristae (Figure 1A-C). Additionally, the 1-year and 2-year representative images show many lipid droplets near mitochondria, which suggest lipid formation as a response to mitochondria stress (Figure 1B-C) [40]. The average area of mitochondria is significantly smaller in samples that are older than 3-month; although the decrease is smaller between the 1-year and 2-year sample (Figure 1D). Although mitochondria become smaller, an inverse effect is seen for mitochondria frequency, as

mitochondria number more than quadruples from the 3-month to 1-year sample, before slightly leveling out from 1-year to 2-year (Figure 1E). Finally, cristae score was used to access cristae of mitochondria. Cristae score is a holistic method to evaluate cristae based on both their quantity and morphology [39,41]. A cristae score of 0 represents no clearly defined cristae, while a cristae of 2 represents that less than 75% of mitochondria have cristae, and a maximum cristae score of 4 represents many regular cristae. Across aging in cardiac muscle, again there was a large drop off in the quality of cristae. The young 3-month sample ranged between mostly regular cristae with some irregular, with cristae scores of about 3.3. The aged samples both have cristae score around 2, which shows there is much area lacking cristae or having irregular cristae. Together, these data suggested that mitochondrial fission increased and cristae regulation decreased across aging; however, TEM can be limiting in analyzing changes of mitochondria, so we moved to a 3D model.

Aging Changes Mitochondria and MERC Morphology in Cardiac Muscle

From there, we sought to determine how aging alters mitochondrial networks and individual mitochondria. We imaged cardiac muscle biopsies from young (3-month-old), mature (1-year-old) and aged (2-year-old) mice by SBF-SEM. While SBF-SEM does not allow for proper viewing of cristae, with resolutions of 10 µm for the x- and y- planes and 50 µm for the z-plane, it allows visualization of the electron connectome [16]. Importantly, it also allows for 3D reconstruction of mitochondria, which more accurately represent how mitochondria exist in 3D space, than 2D methods. We specifically examined the changes of morphology in the intermyofibrillar (IMF) region [42]. While past research has found frequency of mitochondria increases in this reason, further elucidation is needed to show if aging in cardiac muscle changes mitochondria orientation, C-band sarcomeres of myofibrils, or other changes, such as the formation of nanotunnels. We surveyed 175 IMF mitochondria from each of the three mice (n=3) sampled at each time point for SBF-SEM for a total of 500 mitochondria for each age cohort. From there, at 50 µm intervals at the transverse intervals, 300 slices, known as orthos, were sectioned. Given the 10 µm by 10 µm resolution of image stacks, we surveyed approximately 50 IMF mitochondria from each stack.

To begin with analyzing the size and shape of mitochondria, we showcase the orthoslice of the mitochondria showing representative SEM of cardiac muscle (Figure 2A-C), the overlay of the 3D reconstruction (Figure 2A’-C’), and the isolated 3D reconstruction to allow for better viewing of the structure (Figure 2A’’-C’’). We found that there was a significant decrease in perimeter, and volume between the 3 month and 1-year cohorts (Figure 2D-F). In the case of perimeter, 3D area, and volume there was another decrease going from 1-year to 2-year which was a larger increase than the initial decrease in from 3-month (Figure 2D-F). However, in all cases this decrease was less than the decrease present in skeletal muscle we have previously found. Importantly, while the volumes, 3D area, and perimeter of skeletal muscle has previously been shown to be decreased heavily across aging, especially in the 2-year sample, a similar effect was not observed for cardiac muscle (Figure 2D-F). For each of these quantifications, 3 individual mice were sampled at each of the three time points (SFigure 1A-C). When looking at the quantifications of individual mice, most mice were similar and demonstrated a small downward trend, although in some cases the 1-year individuals had higher volume, perimeter, and area than the 3-month young individuals. This suggests that although some mitochondria morphology is loss across aging, less fragmentation has occurred than expected and compared to

other types. From there, we sought to understand if networks of mitochondria changed in response to aging.

To further characterize the changes of cardiac muscle, we looked at them from both a transverse (Figure 3A-C) and longitudinal view (Figure 3A'-C'). They showcased packed together, smaller mitochondria which did not have any significant network formations visible. The mitochondrial branching index has been used in the past as a measure of complexity by examining the ratio between transverse and latitude mitochondria [36]. From there, we did mito-otyping, which is a method similar to karyotyping to organize mitochondria on the basis of their volumes to better categorize the diversity of the mitochondria (Figure 3D).
This allows for comparison of the mitochondria across age at each volume. Critically, it showed that volumes did not have significant changes across all ages, nor did it seem complexity. Furthermore, the decrease in sphericity for cardiac muscle was very small (Figure 3E), so the sphericity barely changed across aging. Similarly, looking at the individual mice for each of the age cohorts, it seems that there is no significant trend (SFigure 2A). In contrast, we have previously found there was a small increase in skeletal muscle sphericity. This suggests that complexity does not significantly increase in cardiac muscle. In combination, the aged cardiac muscle mitochondria resembled healthy mitochondria with a lack of phenotyping or fragmenting present (Figure 3). We further found that in the heart model, in contrast to the skeletal muscle we have previously studied, mitochondria do not develop nanotunnels (Figure 3). While these studies showed mitochondria that managed to maintain their morphology across aging, from there we sought to understand what effects loss of the MICOS complex have on cardiac muscle.

Loss of MICOS Complex Genes across Aging and 3D reconstruction Reveals a Change in Morphology upon their Knockout in Fibroblast

Although it is established that the MICOS complex is critical in mitochondrial dynamics [24,26], the relation to aging requires further elucidation. Previously, *Opa-1* has in the past been found to be decreased across aging [43]. Furthermore, in skeletal muscle we have previously found that *Opa-1*, *Mitofilin*, *Chchd3*, and *Chchd6* significantly decreased across aging; however, we sought to see if the MICOS complex gene transcripts also decreased in cardiac muscle. We found that, as previous research has observed [43], *Opa-1* decreased by over 50% across 2-years compared to the 3-month sample (Figure 4A). *Mitofilin* had a similarly drastic change as the 2-year gene transcript amounts were less than 50% of the 3-month sample (Figure 4B). *Chchd3* and *Chchd6* both also showed a progressive decrease across time, although their levels did not decrease as much as other transcripts (Figure 4C-D). To further understand the role of mitochondrial dynamics upon the loss of these MICOS genes, we knocked them out in fibroblast cells.

Specifically, we measured 1250 mitochondria across 10 cells. Since it is already known that loss of *Opa-1* results in changes in morphology [13,16,17,39], it was a positive control for mitochondrial morphology changes. To begin with, we marked mitochondria with MitoTracker Red and used confocal fluorescence to look to examine mitochondria and verify successful knocking out of *Opa-1*, *Mitofilin*, *Chchd3*, and *Chchd6* (Figure 5A-E). From there, SBF-SEM reconstruction was performed of mitochondria of each of the knockout fibroblasts (Figure 5A'-E'). From there, we performed quantifications for each of the KO models. We saw significant decreases in mitochondria length upon all of the knockouts of the MICOS complex and *Opa-1*

(Figure 5F). Similarly, there were very large decreases in the volume of mitochondria also (Figure 5G). This suggests an uptick in fission potentially in combination with decreased fusion. This is further supported by the much higher percentage of mitochondria that are fragmented (Figure 5H). Notably, *Chchd3* is nearly completely fragmented, similar to *Opa-1*. We further sought to quantify if the mitochondria were more tubular or lamellar, which represents stressed states. We found that while the wildtype was mostly lamellar, all the KO models were much more tubular, with the most tubular being *Opa-1* and *Chchd3*. In combinations, these finds show clear fragmentation and stress states occurring in mitochondria upon the loss of any of the genes associated with the MICOS complex.

DISCUSSION:

Heart failure may be intrinsically linked to mitochondria [4629] and understanding the aging of mitochondria and the role the MICOS complex plays in it is crucial. We demonstrated changes that occur in fibroblasts upon the loss of the MICOS complex. Additionally, we found that while some changes in mitochondria morphology occurs across aging, but, compared to prior studies, less fragmentation occurred.

Importantly, our study combined TEM and SBF-SEM, and was novel in using 3D reconstruction to look at aging cardiac muscle. TEM is an important technique for measuring cristae due to its very high x- and y- resolution [39]. However, it is limited in accurately measuring mitochondria, which are 3D objects that can not be accurately represented in 2D. Therefore, also using SBF-SEM for 3D reconstruction can allow for a more complete understanding of the mitochondria morphology. Future studies may consider also utilizing focused ion beam-scanning electron microscopy, which allows for the 3D reconstruction of smaller objects such as cristae [44]. In the past, FIB-SEM has successfully been performed in mouse muscle to characterize mitochondria [45]. Additionally, mitochondria has been quantified through SBF-SEM in both human and mouse muscles in other studies, such as that by Vincent et al [36]. However, given that cardiac muscle is responsible for the proper contractile of the heart, there remains a gap in the literature in studying it, and our 3D reconstruction begins to elucidate how cardiac muscle changes across aging in a mouse model. This highlighted the importance of further exploring how changes in skeletal muscle specifically affect their form and function through the knockout of the MICOS complex, which we believe may be implicated in aging.

When knocking out the MICOS complex, we saw that the MICOS gene transcripts deteriorated across time (Figure 4). Additionally, we observed in 3D reconstructions that loss of *Opa-1, Mitofilin, Chchd3,* and *Chchd6* resulted in high mitochondrial dysfunction. This was marked by fragmentation, lamellar mitochondria, and much smaller mitochondria (Figure 5). Therefore, it would be expected that since *Opa-1, Mitofilin, Chchd3,* and *Chchd6* are lost over time, their effects on the mitochondria would be felt. However, when we examined the aged model, it was contrary to this in some ways.

Across aging, we observed that mitochondria number increased while the area decreased (Figure 1D-E). This suggests mitochondria fission is increasingly happening, and fusion is happening, mimicking the effects of OPA-1 loss or DRP-1 upregulation [5,17]. However, 3D reconstruction did not show as much fragmentation, with less network formation than the skeletal muscle (Figure 3). Critically, all of the skeletal muscle showed nanotunnels, which are mitochondrial structures which allow for transport of materials and greater mitochondria communication [35]. Although past studies have observed nanotunnels in disease states [35], we

noticed no nanotunnels formed in cardiac muscle, even in aged samples. In cardiac muscle, the mitochondria underwent less fragmenting and less network formation and they did not form nanotunnels (Figure 2-3). We also found lesser complexity in the cardiac mitochondria (Figure 3) and observed that the mitochondria underwent fewer changes with age than we have previously seen in skeletal muscle. It is possible that heart and skeletal muscle respond to aging differently due to differences in nucleation. Skeletal muscles are typically multi-nucleated [11]. As such, even if mitochondria are fragmented, they can still function through the sharing of cellular components. In contrast, heart cells are mono-nucleated. As a result, it may be harder for heart to recover in the loss of mitochondrial efficiency. As such, more resources may be dedicated to ensuring that mitochondria maintain their form, and thus their function in cardiac muscle.

Mitochondria shape may be implicated in heart failure [29], which makes the specific study of cardiac muscle across aging an important therapeutic target. Previously, research has proposed the MFRTA, which speculates that reactive oxygen species alter functions of mitochondria, such as ATP production, to induce aging [50]. As a mechanism to avoid such a mechanism, it is possible the heart ensures more resources to ensuring that mitochondria do not entered stress states, potentially through mitochondria endoplasmic reticulum contacts (MERCs). Future research may consider analyzing MERCs in cardiac muscle to better see how signaling and exchange of calcium changes in stressed mitochondrial states of the heart.

In conclusion, here we combine TEM and 3D reconstructions to evaluate mitochondria and cristae morphology in male mouse cardiac muscle. Specifically, we found that cardiac muscle across aging differentially react compared to prior studies, while the MICOS complex both decreases with age and loss of MICOS complex results in high mitochondrial dysfunction marked by changes in mitochondrial structure. This suggests a potential mechanism that protects cardiac muscle mitochondria from complete fragmentation and formation of nanotunnels in mitochondria, potentially through a mechanism to restore morphology alteration that arose from loss of the MICOS complex. Future studies can explore this mechanism and continue to elucidate the link between age-related heart failure, the MICOS complex, and dysfunction in the mitochondria.

EXPERIMENTAL PROCEDURES

Animal Care and Maintenance

The University of Iowa Animal Care and Use Committee (IACUC) approved all the procedures that were used for care of mice. These protocols are previously described [15] and follow the National Institute of Health Guide for the Care and Use of Laboratory Animals recommendations. WT male C57Bl/6J mice were exclusively used in experiments. They were housed at 22°C on a 12-hour light, 12-hour dark cycle. They had free access to water and standard chow. 5% isoflurane/95% oxygen was used to anesthetize mice.

RNA Extraction and RT-qPCR

Using TRIzol reagent (Invitrogen), RNA was extracted from tissue. From there the RNeasy kit (Qiagen Inc) was used to purify it and it was subsequently quantitated by the absorbance at 260 nm and 280 nm using a NanoDrop 1000 (NanoDrop products, Wilmington, DE, USA) spectrophotometer. Isolated RNA (~1 µg), using a High-Capacity cDNA Reverse Transcription Kit (Applied Biosciences, Carlsbad CA), underwent reverse-transcription. From there, SYBR Green (Life Technologies, Carlsbad, CA) [1] were used to perform real-time quantitative PCR

(qPCR). Three samples for each qPCR (~50 ng) were placed in a 384-well plate that was subsequently underwent qPCR in ABI Prism 7900HT instrument (Applied Biosystems). The specific cycle they underwent was: 1 cycle at 95°C for 10 min; 40 cycles of 95°C for 15 s; 59°C for 15 s, 72°C for 30 s, and 78°C for 10 s; 1 cycle of 95°C for 15 s; 1 cycle of 60°C for 15 s; and one cycle of 95°C for 15 s. Once results were normalized to glyceraldehyde-3-phosphate dehydrogenase (*GAPDH*), data is shown as fold changes. qPCR primers were previously published sequences [15] as shown in Table 1.

Table 1: qPCR Primers Used

Gene	Primers	
Opa-1	Forward	5'-ACCAGGAGACTGTGTCAA-3'
	Reverse	5'-TCTTCAAATAAACGCAGAGGTG-3'
CHCHD3	Forward	5'-GAAAAGAATCCAGGCCCTTCCACGCGC-3'
	Reverse	5'-CAGTGCCTAGCACTTGGCACAACCAGGAA-3'
CHCHD6	Forward	5'-CTCAGCATGGACCTGGTAGGCACTGGGC-3'
	Reverse	5'-GCCTCAATTCCCACATGGAGAAAGTGGC-3'
Mitofilin	Forward	5'-CCTCCGGCAGTGTTCACCTAGTAACCCCTT-3'
	Reverse	5'-TCGCCCGTCGACCTTCAGCACTGAAAACCTAT-3'

CRISPR-Cas9 Knockouts

Adenovirus was used to infect cardiomyocytes to produce the following knockouts—control CRISPR/Cas9 (sc-418922), *CHCHD6* (Mic25) CRISPR (sc-425817), *CHCHD3* (Mic19) CRISPR (sc-425804), and *mitofilin* (Mic60) CRISPR (sc-429376) (Santa Cruz Biotechnology, California, US), with the use of guide RNA (Table 2). For each of the CRISPR 2.5% was combined with 2.5% RNAiMax (ThermoFisher Scientific; 13778075) and the remaning solution was Opti-MEM (Gibco; 31985070) and they were incubated at room temperature for 20 minutes. The media was removed from the cells, and after washing twice with PBS, 200 µL of the CRISPR mixture and 800 µl of Opti-MEM was added to each sample, and they were incubated at 37 C for 4 hours. An additional 1 mL of DMEM medium was added before cells were incubated at 37 C overnight. Cardiocytes were then washed with PBS, and fresh medium was added. After 3 and 7 days, following infection, experiments were performed.

Table 2: Guide RNA and Plasmids Used

Gene Name	Type of Plasmid	CAS Number
Mitofilin	CRISPR/Cas9 KO (m)	sc-429376
CHCHD6	CRISPR/Cas9 KO (m)	sc-425817
CHCHD3	CRISPR/Cas9 KO (m)	sc-425804
Control	CRISPR/Cas9 KO (m)	sc-418922

Serial Block-Face Scanning Electron Microscope (SBF-SEM) Processing of Mouse Muscle Fibers

SBF-SEM was performed as described previously [16,44,46]. 5% isoflurane was used to anesthetize male mice. Hair and skin were removed and cardiac muscle was extracted, cut in 1-mm^3 cubes, and put in 2.5% in 2.5% glutaraldehyde, 1% paraformaldehyde, 120 mM sodium cacodylate solution for 1 hour. From there, 100 mM cacodylate buffer at room temperature was used to wash tissue three times. Tissue was then immersed in 3% potassium ferrocyanide and 2%

osmium tetroxide for 1 hour at 4°C. After this, they were washed with deionized water three times and transferred to 0.1% thiocarbohydrazide and 2% filtered osmium tetroxide and they were incubated for 30 min. Finally, they were again washed with deionized water three times and transferred to 1% uranyl acetate and left overnight at 4°C. The next day, they were washed and samples were transferred to an 0.6% lead aspartate solution for 30 min at 60°C. From there, dehydration was performed by a gradient of five min each in progressively going up, 20%, 50%, 70%, 90%, 95%, and 100% acetone. Cardiac tissues were impregnated in Epoxy Taab 812 hard resin, then moved to new resin, and polymerization occurred at 60°C for 36–48 hours. Blocks of resin were sectioned, cut to 0.5 mm × 0.5 mm, and glued to aluminum pins. These pins were transferred to the FEI/Thermo Scientific Volumescope 2 SEM. 300−400 ultrathin (0.09 µm) serial sections from each of the blocks were collected for conventional TEM. All sections were collected onto formvar-coated slot grids (Pella, Redding CA), stained, and imaged as previously described [16,44,46].

Quantification of TEM Micrographs and Parameters Using ImageJ

The National Institutes of Health (NIH) *ImageJ* software was used for quantification of TEM images, as described previously [39,44]. Each cell of interest was divided into four equal quadrants and half of these quadrants were randomly selected. From those randomly selected, 3 blind individuals measured and quantified them. A minimum of 10 cells were measured by each individual and their findings were then averaged. To verify with accurate and reproducible values, the number of cells analyzed by each individual was increased to 30 if there was high variability.

Segmentation and Quantification of 3D SBF-SEM Images Using Amira

SBF-SEM images were manually segmented in Amira to perform 3D reconstruction, as described previously [16,44]. For each 3D reconstruction, (300−400 slices) were obtained and these were transferred onto Amira. By hand by an individual blind to which samples came from which, structural features were traced manually on sequential slices of micrograph blocks. For each of the 3D reconstructions of cardiac muscle in mice, 30-50 serial sections were chosen at approximately equal z-direction intervals, stacked, aligned, and visualized using Amira to make videos and quantify volumetric structures. 500 total mitochondria across from 3 mice were collected for each quantification. For 3D reconstruction of cardiomyocytes, a minimum of 10 cells were chosen and from them approximately 20 mitochondria from each cell were segmented for a total of about 200 mitochondria. Quantification of 3D structures was performed as described previously [16] using the Amira software (Thermo Scientific). Many parameters were automatically measured by Amira. Algorithms for measurements were entered manually for those not already in the system.

Data Analysis

All SBF-SEM and TEM data were performed in at least three independent experiments and are presented as the mean across these experiments. In presentation, black bars represent the standard error, and dots represent individual data points shown. For data with only two groups, an unpaired, t-test was used. If more than two groups were compared, one-way ANOVA was performed, and significance was assessed using Fisher's protected least significant difference (LSD) test. For both of these analyses, GraphPad Prism software package was used (La Jolla, CA, USA). A minimum threshold of $p < 0.05$ indicated a significant difference. Higher degrees

of statistical significance (**, ***, ****) were defined as $p < 0.01$, $p < 0.001$, and $p < 0.0001$, respectively.

ACKNOWLEDGEMENTS
We would like to thank Mariya Sweetwyne for her advice as an aging expert.

FUNDING
This work was supported by UNCF/BMS EE United Negro College Fund/Bristol-Myers Squibb E.E. T-32, number DK007563 entitled Multidisciplinary Training in Molecular Endocrinology to Z.V.; Just Postgraduate Fellowship in the Life Sciences Fellowship to H.K.B.; NSF MCB #2011577I to S.A.M.; The United Negro College Fund/Bristol-Myers Squibb E.E. Just Faculty Fund, Burroughs Wellcome Fund Career Awards at the Scientific Interface Award, Burroughs Wellcome Fund Ad-hoc Award, National Institutes of Health Small Research Pilot Subaward to 5R25HL106365-12 from the National Institutes of Health PRIDE Program, DK020593, Vanderbilt Diabetes and Research Training Center for DRTC Alzheimer's Disease Pilot & Feasibility Program to A.H.J. Its contents are solely the responsibility of the authors and do not necessarily represent the official view of the NIH. The funders had no role in study design, data collection and analysis, decision to publish, or preparation of the manuscript.

CONFLICT OF INTEREST
The authors declare that they have no conflict of interest.

References:

1. Boudina, S. *et al.* Mitochondrial energetics in the heart in obesity-related diabetes: direct evidence for increased uncoupled respiration and activation of uncoupling proteins. *Diabetes* **56**, 2457–2466 (2007).
2. Brown, D. A. *et al.* Mitochondrial function as a therapeutic target in heart failure. *Nat Rev Cardiol* **14**, 238–250 (2017).
3. Tyumentsev, M. A., Stefanova, N. A., Kiseleva, E. V. & Kolosova, N. G. Mitochondria with Morphology Characteristic for Alzheimer's Disease Patients Are Found in the Brain of OXYS Rats. *Biochemistry Moscow* **83**, 1083–1088 (2018).
4. Alaimo, A. *et al.* Deregulation of Mitochondria-Shaping Proteins Opa-1 and Drp-1 in Manganese-Induced Apoptosis. *PLOS ONE* **9**, e91848 (2014).

5. Lee, Y., Jeong, S.-Y., Karbowski, M., Smith, C. L. & Youle, R. J. Roles of the mammalian mitochondrial fission and fusion mediators Fis1, Drp1, and Opa1 in apoptosis. *Molecular biology of the cell* **15**, 5001–5011 (2004).
6. Zuo, W. *et al.* Mitochondria autophagy is induced after hypoxic/ischemic stress in a Drp1 dependent manner: the role of inhibition of Drp1 in ischemic brain damage. *Neuropharmacology* **86**, 103–115 (2014).
7. Gunter, T. E., Yule, D. I., Gunter, K. K., Eliseev, R. A. & Salter, J. D. Calcium and mitochondria. *FEBS letters* **567**, 96–102 (2004).
8. Mehta, M. M., Weinberg, S. E. & Chandel, N. S. Mitochondrial control of immunity: beyond ATP. *Nat Rev Immunol* **17**, 608–620 (2017).
9. Nicholls, D. G. Mitochondria and calcium signaling. *Cell calcium* **38**, 311–317 (2005).
10. Barja, G. The mitochondrial free radical theory of aging. *Progress in molecular biology and translational science* **127**, 1–27 (2014).
11. Figueiredo, P. A., Mota, M. P., Appell, H. J. & Duarte, J. A. The role of mitochondria in aging of skeletal muscle. *Biogerontology* **9**, 67–84 (2008).
12. Sanz, A. & Stefanatos, R. K. The mitochondrial free radical theory of aging: a critical view. *Current aging science* **1**, 10–21 (2008).
13. Cipolat, S., de Brito, O. M., Dal Zilio, B. & Scorrano, L. OPA1 requires mitofusin 1 to promote mitochondrial fusion. *Proceedings of the National Academy of Sciences* **101**, 15927–15932 (2004).
14. Otera, H., Miyata, N., Kuge, O. & Mihara, K. Drp1-dependent mitochondrial fission via MiD49/51 is essential for apoptotic cristae remodeling. *Journal of Cell Biology* **212**, 531–544 (2016).

15. Pereira, R. O. *et al*. OPA 1 deficiency promotes secretion of FGF 21 from muscle that prevents obesity and insulin resistance. *The EMBO journal* **36**, 2126–2145 (2017).
16. Garza-Lopez, E. *et al.* Protocols for Generating Surfaces and Measuring 3D Organelle Morphology Using Amira. *Cells* **11**, 65 (2022).
17. Frezza, C. *et al.* OPA1 controls apoptotic cristae remodeling independently from mitochondrial fusion. *Cell* **126**, 177–189 (2006).
18. Cogliati, S., Enriquez, J. A. & Scorrano, L. Mitochondrial cristae: where beauty meets functionality. *Trends in biochemical sciences* **41**, 261–273 (2016).
19. Harner, M. E. *et al.* An evidence based hypothesis on the existence of two pathways of mitochondrial crista formation. *eLife* **5**, e18853 (2016).
20. Stephan, T. *et al.* MICOS assembly controls mitochondrial inner membrane remodeling and crista junction redistribution to mediate cristae formation. *The EMBO journal* **39**, e104105 (2020).
21. Mannella, C. A. Consequences of folding the mitochondrial inner membrane. *Frontiers in Physiology* **11**, 536 (2020).
22. Glytsou, C. *et al.* Optic atrophy 1 is epistatic to the core MICOS component MIC60 in mitochondrial cristae shape control. *Cell reports* **17**, 3024–3034 (2016).
23. Eramo, M. J., Lisnyak, V., Formosa, L. E. & Ryan, M. T. The ‘mitochondrial contact site and cristae organising system’ (MICOS) in health and human disease. *The Journal of Biochemistry* **167**, 243–255 (2020).
24. Kozjak-Pavlovic, V. The MICOS complex of human mitochondria. *Cell and tissue research* **367**, 83–93 (2017).

25. Kondadi, A. K. *et al.* Cristae undergo continuous cycles of membrane remodelling in a MICOS-dependent manner. *EMBO reports* **21**, e49776 (2020).

26. Friedman, J. R., Mourier, A., Yamada, J., McCaffery, J. M. & Nunnari, J. MICOS coordinates with respiratory complexes and lipids to establish mitochondrial inner membrane architecture. *Elife* **4**, e07739 (2015).

27. Zhang, J. *et al.* Alterations in mitochondrial dynamics with age-related Sirtuin1/Sirtuin3 deficiency impair cardiomyocyte contractility. *Aging Cell* **20**, e13419 (2021).

28. Parra, V. *et al.* Insulin stimulates mitochondrial fusion and function in cardiomyocytes via the Akt-mTOR-NFκB-Opa-1 signaling pathway. *Diabetes* **63**, 75–88 (2014).

29. Kenny, H. C. & Abel, E. D. Heart Failure in Type 2 Diabetes Mellitus. *Circ Res* **124**, 121–141 (2019).

30. Kim, J., Wei, Y. & Sowers, J. R. Role of mitochondrial dysfunction in insulin resistance. *Circulation research* **102**, 401–414 (2008).

31. Friederich, M., Hansell, P. & Palm, F. Diabetes, oxidative stress, nitric oxide and mitochondria function. *Current diabetes reviews* **5**, 120–144 (2009).

32. Ngoh, G. A., Papanicolaou, K. N. & Walsh, K. Loss of mitofusin 2 promotes endoplasmic reticulum stress. *Journal of Biological Chemistry* **287**, 20321–20332 (2012).

33. Glancy, B., Kim, Y., Katti, P. & Willingham, T. B. The Functional Impact of Mitochondrial Structure Across Subcellular Scales. *Front Physiol* **11**, 541040 (2020).

34. Willingham, T. B., Ajayi, P. T. & Glancy, B. Subcellular Specialization of Mitochondrial Form and Function in Skeletal Muscle Cells. *Front Cell Dev Biol* **9**, 757305 (2021).

35. Vincent, A. E., Turnbull, D. M., Eisner, V., Hajnóczky, G. & Picard, M. Mitochondrial Nanotunnels. *Trends Cell Biol* **27**, 787–799 (2017).

36. Vincent, A. E. *et al.* Quantitative 3D mapping of the human skeletal muscle mitochondrial network. *Cell reports* **26**, 996–1009 (2019).

37. Lesnefsky, E. J., Chen, Q. & Hoppel, C. L. Mitochondrial Metabolism in Aging Heart. *Circ Res* **118**, 1593–1611 (2016).

38. Chaudhary, K. R., El-Sikhry, H. & Seubert, J. M. Mitochondria and the aging heart. *J Geriatr Cardiol* **8**, 159–167 (2011).

39. Lam, J. *et al.* A Universal Approach to Analyzing Transmission Electron Microscopy with ImageJ. *bioRxiv* (2021).

40. Lee, S.-J., Zhang, J., Choi, A. M. K. & Kim, H. P. Mitochondrial dysfunction induces formation of lipid droplets as a generalized response to stress. *Oxid Med Cell Longev* **2013**, 327167 (2013).

41. Eisner, V., Picard, M. & Hajnóczky, G. Mitochondrial dynamics in adaptive and maladaptive cellular stress responses. *Nat Cell Biol* **20**, 755–765 (2018).

42. Vendelin, M. *et al.* Mitochondrial regular arrangement in muscle cells: a “crystal-like” pattern. *American Journal of Physiology-Cell Physiology* **288**, C757–C767 (2005).

43. Tezze, C. *et al.* Age-Associated Loss of OPA1 in Muscle Impacts Muscle Mass, Metabolic Homeostasis, Systemic Inflammation, and Epithelial Senescence. *Cell Metab* **25**, 1374-1389.e6 (2017).

44. Hinton, A. *et al.* A comprehensive approach for artifact-free sample preparation and assessment of mitochondrial morphology in tissue and cultured cells. *bioRxiv* (2021).

45. Glancy, B. *et al.* Mitochondrial reticulum for cellular energy distribution in muscle. *Nature* **523**, 617–620 (2015).

46. Neikirk, K. *et al.* Systematic Transmission Electron Microscopy-Based Identification of Cellular Degradation Machinery. *bioRxiv* (2021).

Figure Legend:

Figure 1: Changes in cardiac muscle mitochondria and cristae across aging revealed in TEM. Representative transmission electron micrographs for cardiac muscle at (**A**) 3-months, (**B**) 1-year (**C**) and 2-years in male mouse skeletal muscle. Quantification of key mitochondria characteristics included (**D**) average mitochondria area, (**E**) the number of mitochondria normalized to the area surveyed, (**F**) and a measurement of the quality of cristae observed. Significance values *, **, ***, **** indicate $p \leq 0.05$, $p \leq 0.01$, $p \leq 0.001$, and $p \leq 0.0001$, respectively.

Figure 2: Changes in cardiac muscle mitochondria morphology across aging revealed in SBF-SEM. (**A-C**) Representative SBF-SEM orthoslice for cardiac muscle. (**A'-C'**) 3D reconstructions of mitochondria in mouse tissues of different ages overlaid on ortho slices. (**A''-C''**) 3D reconstructed and isolated mitochondria for clear visualization. (**D-F**) 3D reconstructions were then quantified. (**D**) Mitochondrial volume in cardiac muscle of different ages. (**E**) Perimeter of the average mitochondria in cardiac muscle. (**F**) 3D area of the average mitochondria in cardiac muscle. Significance values *, **, ***, **** indicate $p \leq 0.05$, $p \leq 0.01$, $p \leq 0.001$, and $p \leq 0.0001$, respectively.

Figure 3: Changes in cardiac muscle branching and networking across aging revealed in TEM. (**A-C**) 3D reconstruction of individually colored mitochondria from a transverse view for mouse cardiac muscle of different ages. (**A'-C'**) 3D reconstruction of individually colored mitochondria from a longitudinal view in cardiac muscle tissues of different ages. (**D**) Mitochondria 3D reconstructions were further organized by volume for each of the age cohorts. (**E**) To measure shape, sphericity changes across aging in cardiac muscle was
Significance value **** indicates $p \leq 0.0001$.

Figure 4: Transcription of *Opa-1* and MICOS genes in aging cardiac muscle.
(A-D) qPCR analyzing the gene transcript fold changes of Opa-1 and MICOS in cardiocytes across aging. (**A**) *Opa-1* transcripts. (**B**) *Mitofilin* transcripts. (**C**) *CHCHD3* transcripts. (**D**) *CHCHD6* transcripts. Significance values *, **, ***, **** indicate $p \leq 0.05$, $p \leq 0.01$, $p \leq 0.001$, and $p \leq 0.0001$, respectively.

Figure 5: (A-D) Confocal fluorescence (using Mitotracker red) shows changes upon individual knockout (KO) of *Opa-1, Mitofilin, Chchd3,* and *Chchd6* in mouse cardiac muscle. (**A'-D'**) Individual KO of *Opa-1, Mitofilin, Chchd3,* and *Chchd6* was also observed in 3D reconstruction of SBF-SEM. (**E-G**) Quantification upon KO-state of each MICOS gene and *Opa-1* was performed in 3D reconstruction. (**E**) Mitochondria length and (**F**) mitochondria volume decreased upon each KO. (**G**) Additionally, the relative frequency of mitochondria that presented

as fragmented was increased across KO of the MICOS genes and *Opa-1* while tubular mitochondria decreased.

Supplementary Figure 1. Individual quantifications for (**A**) average volume per mitochondria, (**B**) average 3D area of mitochondria, and (**C**) average perimeter of the mitochondria for each of the three mice sampled at 3-months, 1-year, and 2-years.

Supplementary Figure 2. (**A**) For sphericity, all three mice sampled at each time point had similar sphericity values that stayed mostly consistent across time.

Figure 1

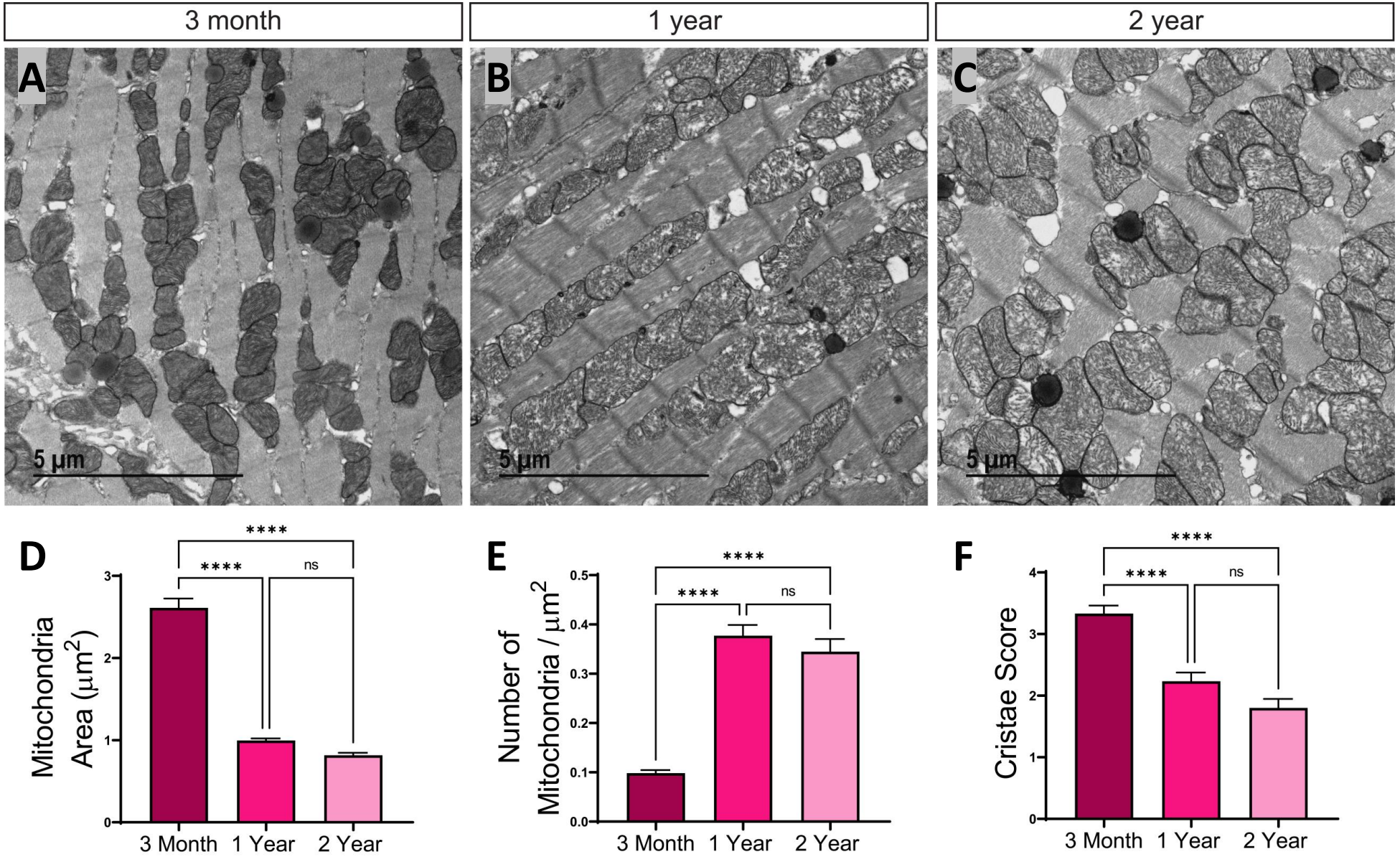
3 month
1 year
2 year
A
B
C
5 µm
5 µm
5 µm
D
Mitochondria Area (µm2)
****
****
ns
3 Month
1 Year
2 Year
E
Number of Mitochondria / µm2
****
****
ns
3 Month
1 Year
2 Year
F
Cristae Score
****
****
ns
3 Month
1 Year
2 Year

Figure 2

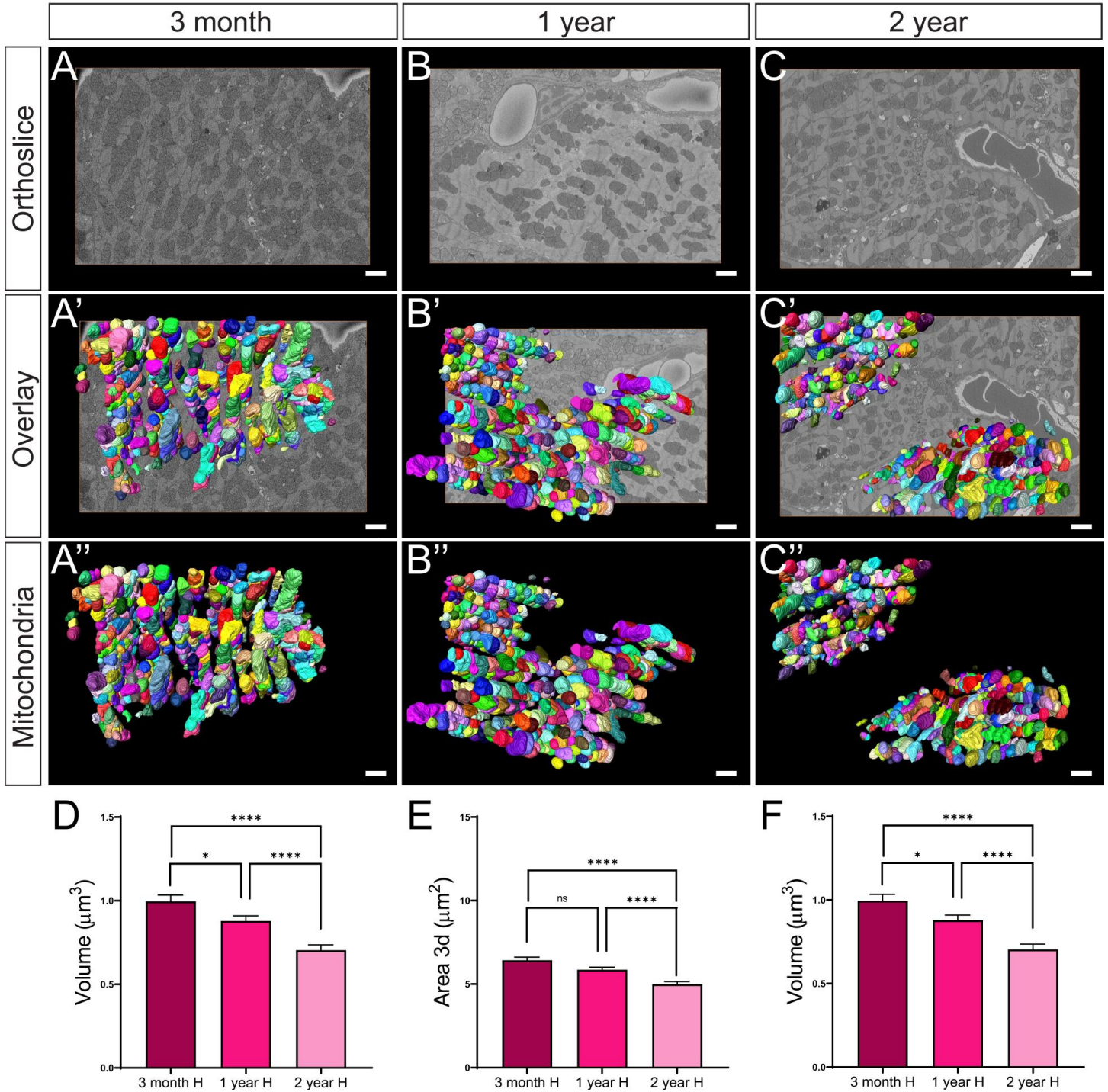
3 month
1 year
2 year
Orthoslice
Overlay
Mitochondria
A
B
C
A'
B'
C'
A''
B''
C''
D
E
F
Volume (μm3)
Area 3d (μm2)
1.5
1.0
0.5
0.0
15
10
5
0
****
*
ns
3 month H
1 year H
2 year H

Figure 3

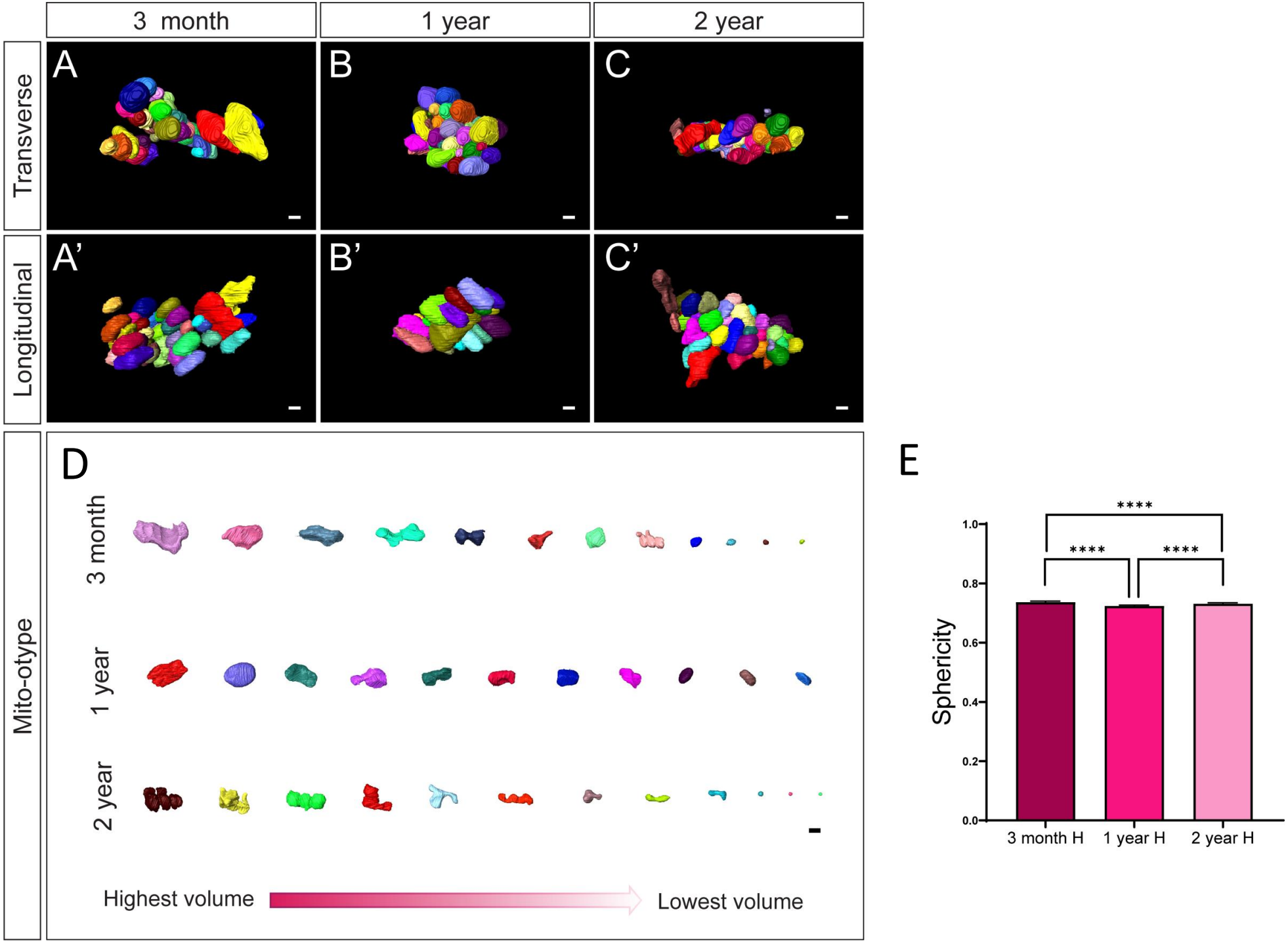
3 month
1 year
2 year
Transverse
Longitudinal
Mito-otype
A
B
C
A'
B'
C'
D
3 month
1 year
2 year
Highest volume
Lowest volume
E
Sphericity
1.0
0.8
0.6
0.4
0.2
0.0
****
****
****
3 month H
1 year H
2 year H

Figure 4

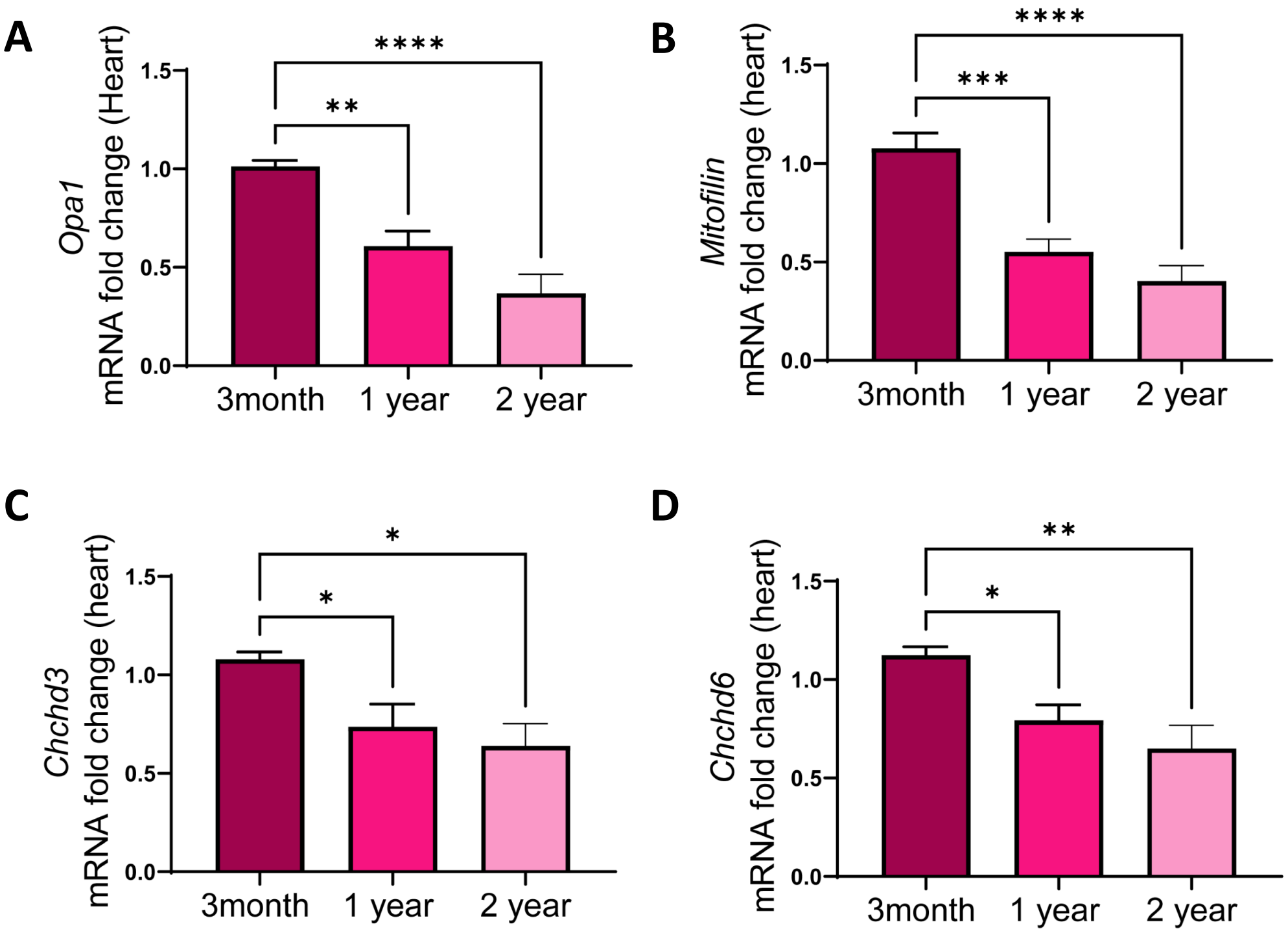
A
Opa1
mRNA fold change (Heart)
1.5
1.0
0.5
0.0
****
**
3month
1 year
2 year
B
Mitofilin
mRNA fold change (heart)
1.5
1.0
0.5
0.0
****
***
3month
1 year
2 year
C
Chchd3
mRNA fold change (heart)
1.5
1.0
0.5
0.0
*
*
3month
1 year
2 year
D
Chchd6
mRNA fold change (heart)
1.5
1.0
0.5
0.0
**
*
3month
1 year
2 year

Figure 5

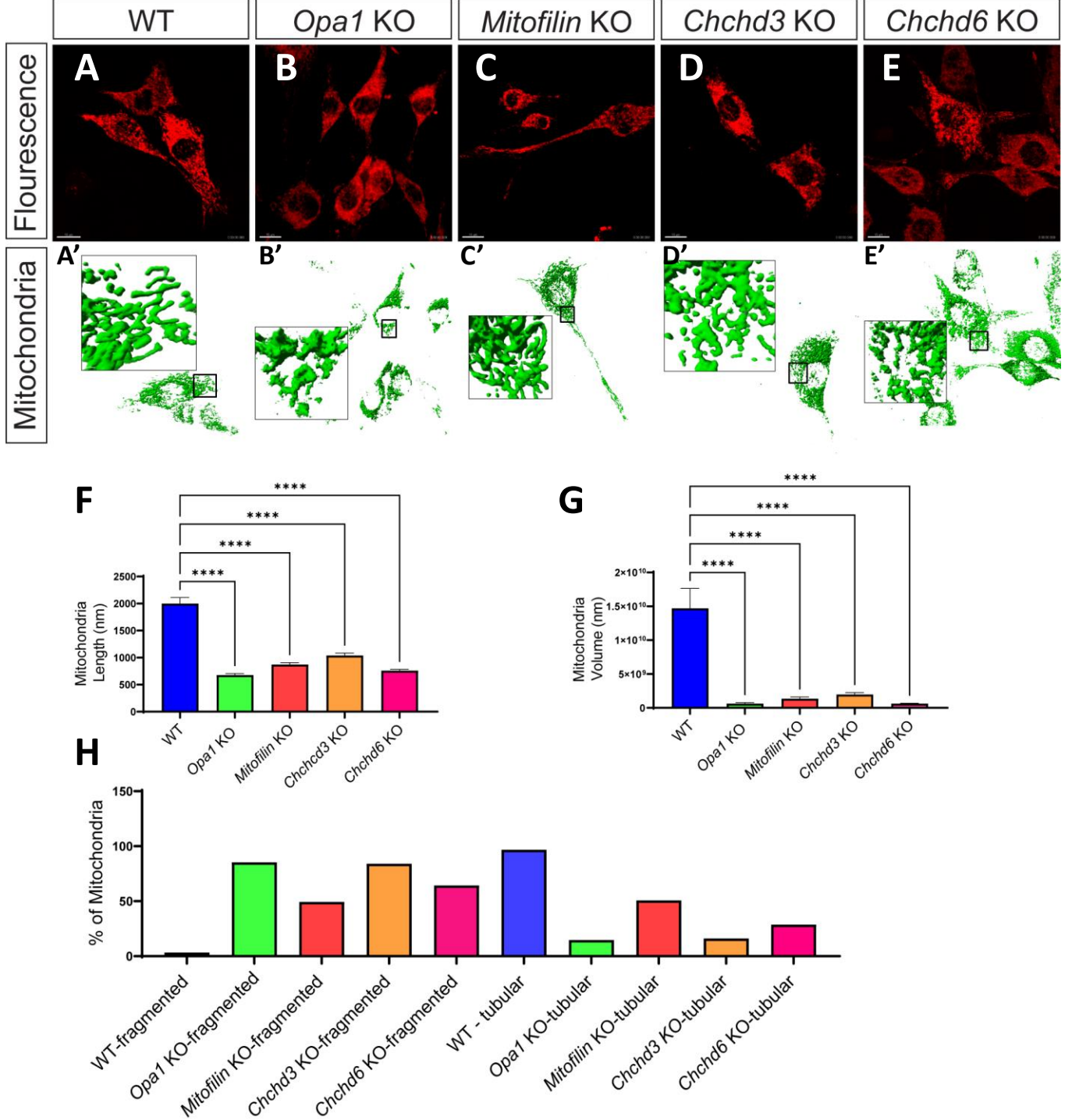
WT
Opa1 KO
Mitofilin KO
Chchd3 KO
Chchd6 KO
Flourescence
Mitochondria
A
B
C
D
E
A'
B'
C'
D'
E'
F
Mitochondria Length (nm)
2500
2000
1500
1000
500
0
****
WT
Opa1 KO
Mitofilin KO
Chchd3 KO
Chchd6 KO
G
Mitochondria Volume (nm)
2×10¹⁰
1.5×10¹⁰
1×10¹⁰
5×10⁹
0
H
% of Mitochondria
150
100
50
0
WT-fragmented
Opa1 KO-fragmented
Mitofilin KO-fragmented
Chchd3 KO-fragmented
Chchd6 KO-fragmented
WT - tubular
Opa1 KO-tubular
Mitofilin KO-tubular
Chchd3 KO-tubular
Chchd6 KO-tubular